ISSN 1027-5495. Functional Materials, 28, No.3 (2021), p. 469-474.
doi:https://doi.org/10.15407/fm28.03.469

Preparation of polyaniline/manganese dioxide nanocomposites by *in situ* polymerization method and their conductivity properties

***S.C.Vella Durai*[1], *R.Indira*[2], *E.Kumar*[3]**

[1]Department of Physics, JP College of Arts and Science, Agarakattu, Tenkasi, Tamilnadu, India
[2]PG Department of Chemistry, SDNB Vaishnav College for Women, Chromepet, Chennai. Tamilnadu, India
[3]School of Science, Department of Physics, Tamil Nadu Open University, Chennai. Tamilnadu, India

Received December 25, 2020

The polyaniline /manganese dioxide nanocomposite (PANI/MnO_2) was prepared by *in situ* polymerization. The structural, electrical conductivity, complex electric modulus, dielectric and optical properties of the nanocomposites were analyzed using powder XRD, impedance and optical spectra. After heating of PANI/MnO_2 nanocomposites, XRD shows structure changes to an extremely less crystalline state due to the melting of MnO_2, which is inside the PANI chain. The AC conductivity of nanocomposites was analyzed in the range from 298 K to 423 K. The AC conductivity of nanocomposites varies with frequency. The highest conductivity is 5.798 Ohm/cm at a temperature of 373 K. The dielectric permittivity is constant in the region of higher frequencies and differs in the region of lower frequencies. Studies of FTIR spectra have shown that there is a very strong interaction between MnO_2 and the PANI chain.

Keywords: conductivity, dielectric, modulus, optical, structural.

Отримання нанокомпозитів поліанілін/діоксид марганцю методом полімеризації *in situ* і їх характеристики провідності. *S.C.Vella Durai, R.Indira, E.Kumar*

Нанокомпозит поліанілін/діоксид марганцю (PANI/MnO_2) отримано методом полімеризації *in situ*. Структуру, електропровідність, комплексний електричний модуль, діелектричні і оптичні властивості нанокомпозитів проаналізовано за допомогою порошкового XRD, імпедансу і оптичних спектрів. XRD після нагрівання нанокомпозитів PANI/MnO_2 показує, що структура змінюється на виключно менш кристалічну через плавлення MnO_2, який знаходиться всередині ланцюга PANI. Провідність нанокомпозитів за змінним струмом проаналізовано у діапазоні від 298 К до 423 К. Показано, що вона змінюється в залежності від частоти. Найбільша провідність становить 5,798 Ом/см при температурі 373 К. Діелектрична проникність постійна в області більш високих частот і розрізнялася в області більш низьких частот. Дослідження інфрачервоних спектрів з перетворенням Фур'є показали, що існує дуже сильна взаємодія між MnO_2 і ланцюжком PANI.

Нанокомпозит полианилин/диоксид марганца (PANI/MnO_2) получен методом полимеризации *in situ*. Структура, электропроводность, комплексный электрический модуль, диэлектрические и оптические свойства нанокомпозитов проанализированы с помощью порошковой XRD, импеданса и оптических спектров. XRD после нагрева нанокомпозитов PANI/MnO_2 показывает, что структура меняется на менее кристаллическую из-за плавления MnO_2, который находится внутри цепи PANI. Проводимость

нанокомпозитов по переменному току проанализирована в диапазоне от 298 К до 423 К. Проводимость нанокомпозитов по переменному току меняется в зависимости от частоты. Наибольшая проводимость составляет 5,798 Ом/см при температуре 373 К. Диэлектрическая проницаемость постоянна в области более высоких частот и различалась в области более низких частот. Исследования инфракрасных спектров с преобразованием Фурье показали, что существует очень сильное взаимодействие между MnO_2 и цепочкой PANI.

1. Introduction

Conducting polymers such as, polyaniline (PANI) can be used for better conductivity with certain organic material, which makes it widely used in sensors, vessels, and chemical catalysis [1–3]. MnO_2 has attracted great interest as an environmentally friendly metal oxide for lithium battery, sensor, catalyst, and electrochemical capacitor applications [4, 5]. Polymer based nanocomposites have good potential applications like sensors, etc. [6, 7]. In order to obtain high performance, aniline have been polymerized with some other material, from which polyaniline/Au, polyaniline/carbon, polyaniline/graphene, and others have been prepared by [1, 2]. Meanwhile, to improve the characteristics of the supercapacitors, 50/50 composites were additionally fabricated, consisting of MnO_2 and various materials [8, 9]. Different techniques of preparing PANI/MnO_2 composites were discussed [10]. Considering the choice of reaction, crystal size and agglomeration associated with the nanostructure, it is expected that the main problems will be associated with improving efficiency; and widespread use is based on the controlled production of an improved crystal structure [11]. With regard to the preparation of polyaniline, a physicochemical technique was recommended [12], in which the simple interfacial polymerization method is a very flexible approach without any template. The oxidant is separated out from the organic solution, while the reaction occurs at the interfaces. As the product is removed from the prepared bulk solution, a new polymerization step occurs at the interfaces with the desired PANI growth, at which the size and shape of the product can be controlled. In addition, prepared MnO_2 is extensively used. With minimal cost and material availability, the best properties of MnO_2, PANI, and PANI/MnO_2 nanocomposites are widely analyzed.

In this work, PANI/ MnO_2 nanocomposite with controllable crystalline size has been prepared by means of *in situ* polymerization methods, which exhibits good conductivity. The PANI nanocomposite allows crystalline MnO_2 nanoparticles to scatter. In this paper, the structural features and the AC conductivity of the nanocomposites were investigated. In previous papers, the preparation of 1 wt.%, 5 wt.% and 10 wt.% of PANI/MnO_2 nanocomposites was discussed [13, 14]; and they showed significant changes in conductivity compared to pure materials. In this paper, detail analyzes of 2 wt.% of PANI/MnO_2 nanocomposites are discussed. The AC impedance spectra method is a very powerful tool to study the electrical and dielectric properties of the prepared new composite materials. This paper also reported on studies of the dielectric and electrical moduli of PANI/MnO_2 nanocomposites.

2. Experimental

2.1 Preparation of PANI/MnO_2 nanocomposites

PANI/MnO_2 (2 wt%) nanocomposites were prepared by *in situ* polymerization of aniline with synthesized MnO_2 nanoparticles using ammonium persulfate as an oxidant. 0.1 M aniline was added drop by drop to 2 M HCl solution and the mixture was kept in a magnetic stirrer for 40 min at 50°C. Ammonium persulfate was dissolved in 2 M HCl solution mixture and stirred for 2 h. Then both the mixtures were added to the synthesized MnO_2 nanoparticles (2 % w/v). The solution mixture was stirred continuously for 50 min. The reaction was completed by the formation of colloidal green solution. PANI/MnO_2 nanocomposites obtained were cooled and dried for one week. The dried nanocomposites were grounded into powder.

2.2 Characterizations

The structure of the PANI/MnO_2 nanocomposite was investigated by powder XRD technique and the data were recorded using an X-ray diffractometer (Model Bruker D8) with nickel filtered Cu–Kα radiation. The samples were characterized using impedance spectroscopy. An impedance bridge (Zahner IM6) was used to measure the dielectric, modulus, and *ac* conductivity at several frequencies in the range of 10 μHz to 8 MHz (at different temperatures). The FTIR spec-

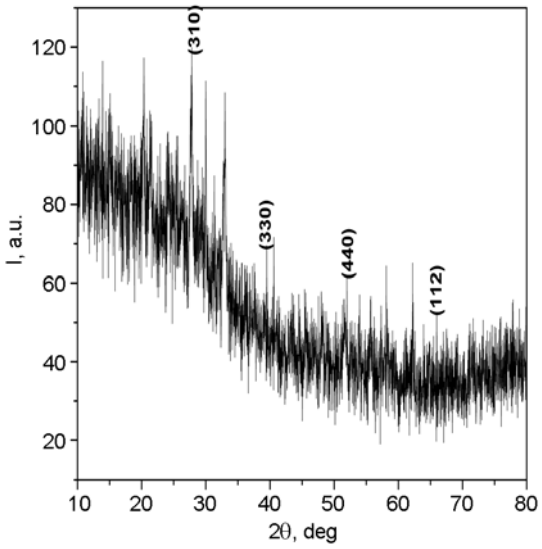

Fig. 1. XRD patterns of nanocomposites.

trum of the MnO_2 powder sample was also recorded using Fourier Transform Infra-Red spectroscopy (FTIR) (JASCO FTIR-4100).

3. Results and discussion

3.1 Powder XRD analysis

Powder XRD studies were used to investigate the structure of the PANI/MnO_2 nanocomposite. Figure 1 shows a powder X-ray diffraction pattern of the PANI/MnO_2 nanocomposite; the diffraction peaks of pure PANI [15] and its nanocomposite are observed at diffraction angles $2\theta = 27$, 39, 52, and 66 degrees due to a certain perpendicular and parallel interval of the polyaniline chain. The diffraction peaks at $2\theta = 27$, 30, and 33 deg corresponding to d spacings of 3.21139 Å, 2.97687 Å, and 2.71208 Å, respectively, show fine-crystalline structure of the nanocomposite. In addition, the crystallite size of nanocomposites is $D = 18$ nm, calculated using the Scherer equation [16]. It confirms the presence of MnO_2 nanoparticles, and also shows an increase in crystallite size of 2 wt.% PANI/MnO_2 nanocomposites. According to Fig. 4, peaks recorded at $2\theta = 27$, 39, 52 and 66 degrees from (310), (330), (440) and (112) planes, respectively, are shifted; but there is an increase in 2 wt.% MnO_2 nanoparticles in PANI/MnO_2 nanocomposites. This indicated the presence of nano-crystalline phases in the synthesized nanocomposite materials. The XRD pattern confirms the results of previous articles describing the effect of MnO_2 nanoparticles in PANI/MnO_2 nanocomposites. As expected, 2 wt.% MnO_2 nanoparticles have considerable effect on incorporation of PANI, as they can make change in properties of this polymer.

3.2 Electric modulus analysis

One more studies of the complex electric modulus behaviour may be discussed by the modulus formulations, which suppress the effect of the electrodes polarization [17]. The modulus at different temperatures is shown in Fig. 2a and b, for (2 wt.%) polymer based nanocomposite, respectively. At low frequencies, the imaginary and real parts of the electrical modulus approach zero, which indicates that the polarization of the electrodes makes a negligible contribution [18]. The continuous constant at low frequency region is due to the good capacitance related with the electrode materials

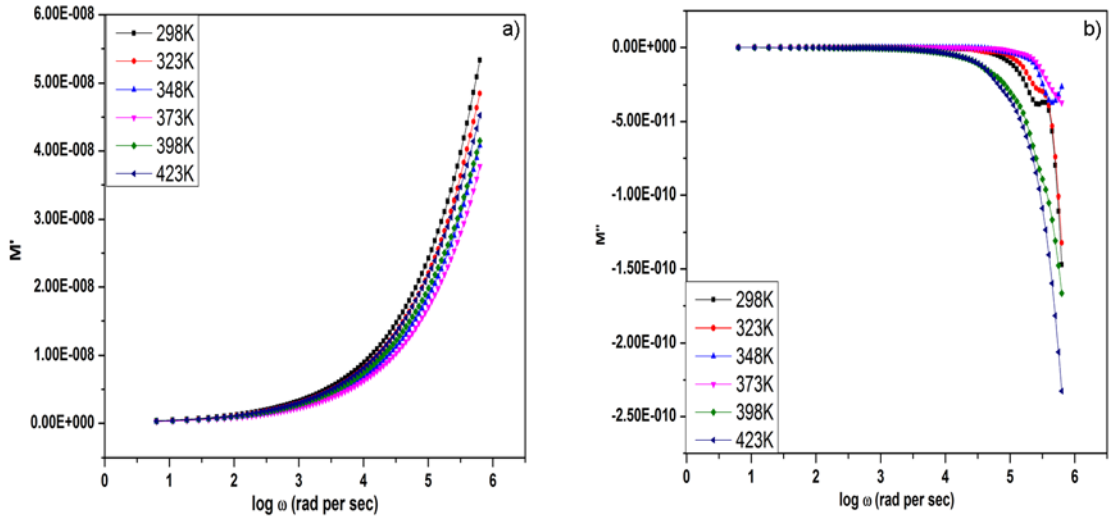

Fig. 2. a) Variation of Modulus (real) with frequency at different temperatures, b) variation of Modulus (imaginary) with frequency at different temperatures.

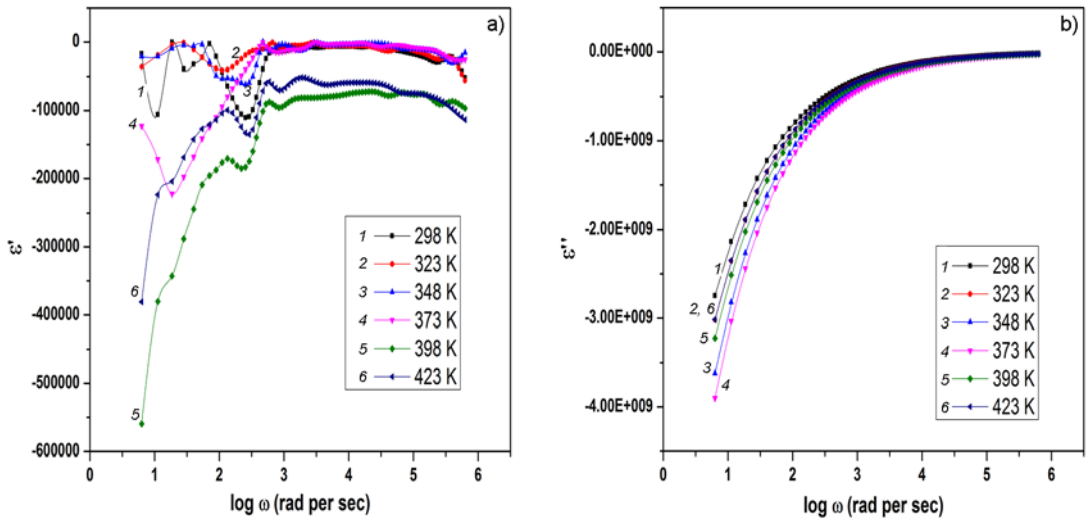

Fig. 3. a) Variation of dielectric constant (real) with frequency at different temperatures, b) variation of dielectric constant (imaginary) with frequency at different temperatures.

[19]. The presence of peaks in the formalism of the imaginary modulus at high frequencies for the polymer based electrolyte materials indicates that ionic conduction is pre-dominant in the polymer based electrolytes. As the frequency increases in the real modulus, the peaks shift to higher frequencies, but with increasing frequency in the imaginary modulus, the peaks also shift to higher frequencies.

3.3 Analysis of dielectric properties

The (ε^*) dielectric constant is obtained by $\varepsilon^* = \varepsilon' - i\,\varepsilon''$, where ε'' is the imaginary part of the dielectric constant, ε' is the real part of dielectric constant. Dielectric constant (dielectric permittivity) is a direct observable measure of dissipated energy and is related to ion motion as well as charge polarizations [20]. The plot of angular frequency versus real and imaginary dielectric constants for 2 wt.% of PANI/MnO_2 nanocomposites at different temperatures are given in Fig. 3a and b, respectively. The dielectric permittivity (ε' & ε'') becomes very large and constant at a higher frequency region (3 to 6 rad/s) due to the free movement of the charge in the material [21]. This value does not correspond to the pure materials. For lower frequency region (0.5 to 3 rad/s), a continuous change in ε'' and ε' is observed. This phenomenon is explained by the so called conductivity relaxations [22].

The appearance of both dielectric peaks shows that the frequency region changes from maximum to lower with increasing temperature. It can be seen from the figures that the rapid decrease in the dielectric constant at low frequencies is explained by the contribution of the space charge. By applying the electric field, the charge carriers migrate from the grain and accumulated at grain boundaries. This can occur at high polarization and, therefore, a high dielectric constant [23] manifests itself at lower frequencies. In the high-frequency region, due to the high periodic change in the direction of the field at the interface, the contribution of charge carriers (ions) to the dielectric constant remains constant with increasing frequency [24]. In the synthesized nanocomposite materials, the polarization decreases due to the accumulation of charges and leads to a decrease in the value of real dielectric constant (ε').

3.4 Electrical conductivity analysis

The AC conductivity of the polymer based nanocomposites is characterized with respect to the angular frequency. Plots of conductivity versus logarithmic angular frequency for mixed polymer nanocomposites show good PANI/MnO_2 conductivity at various temperatures, as shown in Fig. 4. The ionic conductivity of the synthesized materials was realized when the ion moved along the hopping mechanism between the allowed sites [25]. For more conductors, the AC conductivity usually reaches a frequency-independent plot. In crystalline ionic materials, some dispersion of AC conductivity was observed in both the low-frequency and high-frequency regions. The data obtained for the synthesized nanocomposites show (Fig. 4) that the frequency dependence of AC conductivity explains the dispersion in both (high and low) frequency ranges. The AC conductivity (σ_{ac}) of the synthesized nano-

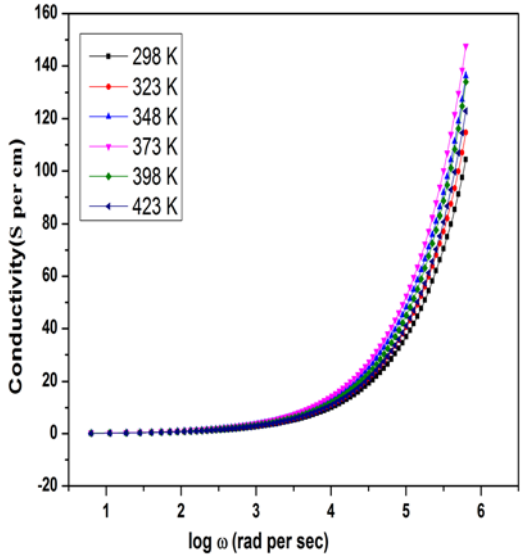

Fig. 4. Log ω *Vs ac* conductivity of nanocomposites at different temperatures.

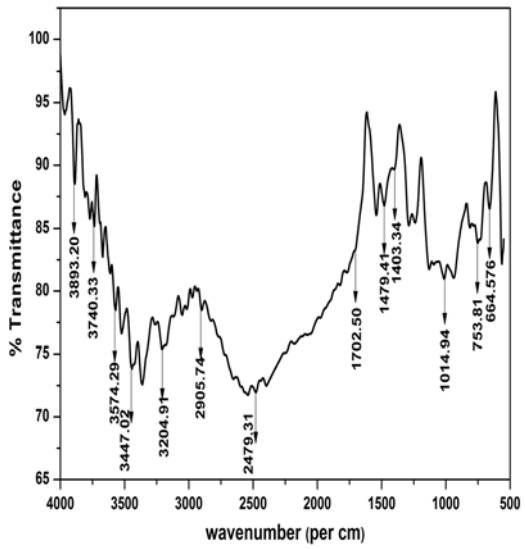

Fig. 5. FT-IR spectra of nanocomposites.

composite was calculated using the below formula,

$$\sigma_{ac} = \varepsilon_0 \varepsilon_r \omega \tan\delta, \quad (1)$$

where ε_0 is the permittivity ($8.85 \cdot 10^{-12}$ F/m for free space), ω is the angular frequency, ε_r is the dielectric constant and tanδ is the loss factor. The plot of AC conductivity changes as a function of logarithmic angular frequency for nanocomposites and shows a high electrical conductivity at different temperatures (Fig. 4). In the low frequency regions, the AC conductivity is found to be constant with an increase in temperature. In the middle angular frequency range, the AC conductivity plot was found to be independent on the angular frequency. At high angular frequencies, the AC conductivity was found to increase with increasing temperature. Therefore, it has been observed that AC conductivity is highly frequency dependent and appears to be high at higher frequencies.

3.5 FTIR analysis

The FTIR spectra depict the formation of PANI/MnO_2 nanocomposites and organic build-up on the outside of MnO_2 nanoparticles. Fig. 5 shows the FTIR spectrum of PANI\MnO_2 (2 wt.%) nanocomposites. The peak at 664 cm^{-1} is the extended vibration peak of Mn–O. The peaks at 1479.41, 1403.34, 1014.94 and 753.81 cm^{-1} correspond to PANI [26]. The peak at 1479.41 cm^{-1} is attributed to the stretching vibration of the benzoic (-(CH_4)-) ring [27]. The peaks observed at 1014.94 cm^{-1} correspond to the stretching of C–H in-plane and out-of-plane bending. The N–H stretching vibration mode appears at 3000 cm^{-1}. In addition, the peaks at 3204.91 and 3447.02 cm^{-1} for N–H (PANI) and O–H (H_2O), respectively, are observed [27]. The peak near 3400 cm^{-1} (O–H) became intense with decreasing acid concentration, which revealed the presence of hydrated MnO_2. Based on the observations of FTIR spectra, the presence of this component in the nanocomposite is confirmed. The absorption peaks of the PANI/MnO_2 nanocomposite appear for both PANI and MnO_2, demonstrating the presence of both components in the nanocomposites.

4. Conclusions

The polymer based nanocomposites have been synthesised by *in situ* polymerization method. The fine-crystalline nature of the nanocomposites was confirmed by powder XRD. Maximum conductivity of 5.798 Ω/cm was measured for nanocomposites at 373 K. Low values of real dielectric permittivity varied at low frequencies and were constant at high frequencies. Low values of imaginary dielectric permittivity varied in the low frequency region and constant at high frequencies. The values of real and imaginary electric modulus were found to be constant in the low frequency region. The structure of the synthesized nanocomposite was studied by FTIR spectra. This article presents a new method for the synthesis of

various types of polymer/metal oxide nanocomposites.

References

1. K.Wang, J.Huang, Z.Wei, *J. Phys. Chem. C*, **8**, 8062 (2010).
2. K.Zhang, L.L.Zhang, X.S.Zhao, J.Wu, *Chem. Mater.*, **8**, 1392 (2010).
3. J.Huang, S.Virji, B.H.Weiller, R.B.Kaner, *J. Am. Chem. Soc.*, **8**, 314 (2003).
4. L.Athouel, F.Moser, R.Dugas et al., *J. Phys. Chem. C*, **8**, 7270 (2008).
5. S.Devaraj, N.Munichandraiah, *J. Phys. Chem. C*, **8**, 4406 (2008).
6. O.P.Olasyuk, O.P.Dmytrenko, M.P.Kulish et al., *Functional Materials*, **24**, 563 (2017).
7. Chen Jian-bing, Li Zhun-zhun, Xu Nan, *Funct. Mater.*, **25**, 93 (2018).
8. J.W.Long, M.B. Sassin, A.E.Fischer, D.R.Rolison, *J. Phys. Chem. C*, **8**, 17595 (2009).
9. S.Chen, J.Zhu, X.Wu et al., *ACS Nano.*, **8**, 2822 (2010).
10. F.J.Liu, *Synth. Met.*, **8**, 1896 (2009).
11. R.G.Chaudhuri, S.Paria, *Chem. Rev.*, **8**, 2373 (2012).
12. H.X.He, C.Z.Li, N.Tao, *J. Appl. Phys. Lett.*, **8**, 811 (2001).
13. S.C.Vella Durai, E.Kumar, *J. Ovonic Res.*, **16**, 173 (2020).
14. E.Kumar, S.C.Vella durai, L.Guru Prasad et al,, *J. Mater. Environ. Sci.*, **8**, 3490 (2017).
15. A.Mostafaei, A.Zolriasatein, *Prog. Nat. Sci.:Mater. Int.*, **22**, 273 (2012).
16. S.C.Vella Durai, E.Kumar, D.Muthuraj, V.Bena Jothy, *J. Nano-Electron. Phys.*, **12**, 03011 (2020).
17. S.F.Cherif, A.Cherif, W.Dridi, M.F.Zid, *Arabian J. Chem.*, **13**, 5627 (2020).
18. H.Nithya, S.Selvasekarapandian, D.Arun Kumar et al., *Mater. Chem. Phys.*, **126**, 404 (2011).
19. R.Mishra, N.Baskaran, P.A.Ramakrishnan, K.J.Rao, *Solid State Ionics*, **112**, 261 (1998).
20. K.A.Mauritz, *Macromolecules*, **22**, 4483 (1989).
21. A.Kyritsis, P.Pissis, J.Grammatikakis, *J. Polym, Sci. Part B : Polym. Phys.*, **33**, 1737 (1995).
22. J.Malathi, M.Kumaravadivel, G.M.Brahmanandhan et al., *J. Non-Cryst. Solids*, **356**, 2277 (2010).
23. K.Dutta, S.K.De, *J. Appl. Phys.*, **102**, 084110 (2007).
24. H.Nithya, S.Selvasekarapandian, P.Christopher Selvin et al., *Electrochim. Acta*, **66**, 110 (2012).
25. S.Selvasekarapandian, M.Vijayakumar, *Mater. Chem. Phys.*, **80**, 29 (2003).
26. S.Vijayalakshmi, *Intern. J. Engin. Res. Computer Sci. Engin.*, **5**, 750 (2018).
27. Fanhui Meng, Xiuling Yan, Ye Zhu, Pengchao Si, *Nanoscale Res. Lett.*, **8**, 179 (2013).